Summertime response of ozone and fine particulate matter to mixing layer meteorology over the North China Plain

Jiaqi Wang[1], Jian Gao[1], Fei Che[1], Xin Yang[1], Yuanqin Yang[2], Lei Liu[2], Yan Xiang[3]

[1]State Key Laboratory of Environmental Criteria and Risk Assessment, Chinese Research Academy of Environmental Sciences, Beijing 100012, China

[2]State Key Laboratory of Severe Weather and Key Laboratory for Atmospheric Chemistry of CMA, Chinese Academy of Meteorological Sciences, Beijing 100081, China

[3]Institutes of Physical Science and Information Technology, Anhui University, Hefei, China

Correspondence to: Jian Gao (gaojian@craes.org.cn)

Abstract. Measurements of surface ozone (O_3), $PM_{2.5}$ and its major secondary components (SO_4^{2-}, NO_3^-, NH_4^+, and OC), mixing layer height (MLH) and other meteorological parameters were made in the North China Plain (NCP) during warm seasons (June–July) in 2021. The observation results showed that the summertime regional MDA8 O_3 initially increased and reached the maximum (195.88 μg m^{-3}) when MLH at around 900–1800 m, then turned to decrease with further evolution of MLH. Interestingly, synchronized increases in $PM_{2.5}$ concentration along with the development of the mixing layer (MLH < 1200 m) have been witnessed, and the positive response of $PM_{2.5}$ to MLH was significantly associated with the increase in SO_4^{2-} and OC. It was found that this increasing trend of $PM_{2.5}$ with elevated MLH was not only determined by the effect of wet deposition process but also by the enhanced secondary chemical formation, which was related to appropriate meteorological conditions (50 % < RH < 70 %) and increased availability of atmospheric oxidants. Air temperature played a minor role in the change characteristics of $PM_{2.5}$ concentration, but greatly controlled the opposite change characteristics of SO_4^{2-} and NO_3^-. The concentrations of $PM_{2.5}$ and its major secondary components, as well as SOR and NOR, increased synchronously with elevated MDA8 O_3 concentration, and the initial increase of $PM_{2.5}$ along with the increased MLH corresponded well with that of MDA8 O_3. We highlight that the correlation between MLH and secondary air pollutants should be treated with care in hot seasons, and the superposition-composite effects of $PM_{2.5}$ and O_3 along with the evolution of mixing layer should be considered when developing $PM_{2.5}$-O_3 coordinated control strategies.

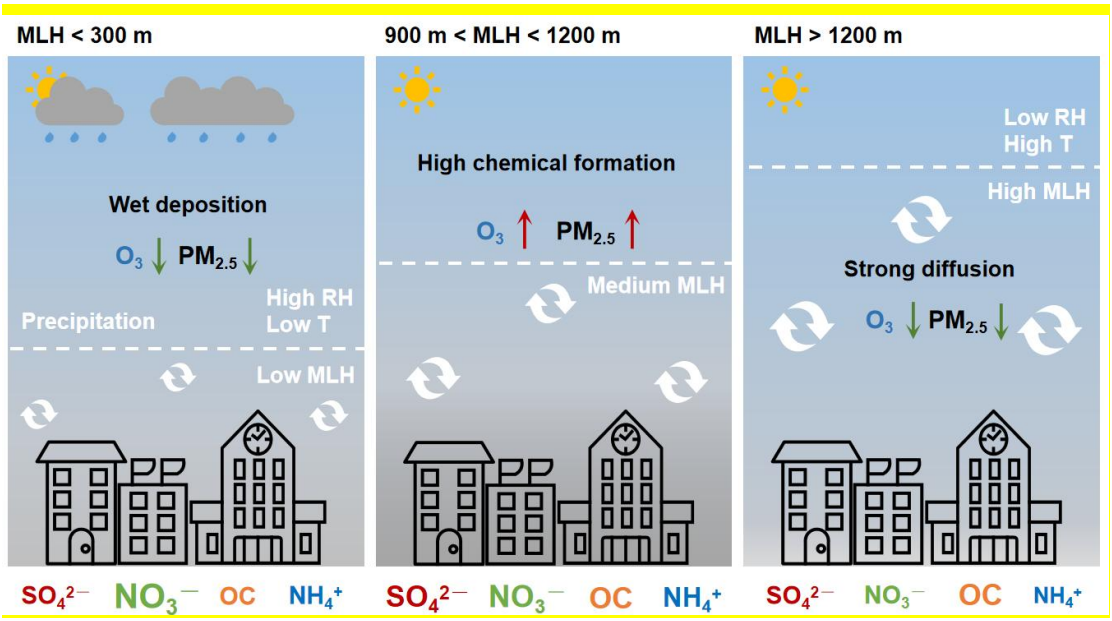
MLH < 300 m
Wet deposition
O3 PM2.5
Precipitation
High RH
Low T
Low MLH
SO4 2− NO3 − OC NH4 +
900 m < MLH < 1200 m
High chemical formation
O3 PM2.5
Medium MLH
SO4 2− NO3 − OC NH4 +
MLH > 1200 m
Low RH
High T
High MLH
Strong diffusion
O3 PM2.5
SO4 2− NO3 − OC NH4 +

31

32

1 Introduction

Surface ozone (O_3) and $PM_{2.5}$ (atmospheric fine particles with an aerodynamic diameter of less than 2.5 μm) are important air pollutants in the atmosphere and have aroused a lot of attention from the public due to their adverse health impact (Jiang et al., 2018; Cohen et al., 2017; Gao and Ji, 2018). Even though stringent clean air actions have been implemented in China during the past decade, high concentrations of O_3 and/or $PM_{2.5}$ exceeding the national air quality standards still occurred during warm seasons (June–August) in China, especially in the North China Plain (NCP), the economic center of China (Dai et al., 2023). O_3 is a secondary pollutant originated from photochemical oxidation of volatile organic compounds (VOC) and carbon monoxide (CO) in the presence of nitrogen oxides (NO_X), and $PM_{2.5}$ is mainly determined by the atmospheric processes of emissions and secondary formation from gaseous precursors. In addition to air pollutant emissions, meteorological conditions play critical roles in the formation of $PM_{2.5}$ and O_3 (Miao et al., 2021). Mixing layer height (MLH), which influences the vertical mixing within the pollution mixing layer and determines the dilution of pollutants emitted near the ground (Haman et al., 2014; Zhu et al., 2018; Lou et al., 2019), often serves as a critical physical parameter in atmospheric environmental evaluation. Elucidating the association of MLH with surface O_3 and $PM_{2.5}$ is fundamental for the development of $PM_{2.5}$-O_3 coordinated control strategies.

The response of air pollution to MLH was changeable and complicated (Miao et al., 2021). Previous works frequently assumed that the narrowing of mixing layer resulted in accumulation of pollutants near the ground and the increase in MLH was expected to reduce $PM_{2.5}$ concentration due to dilution (Murthy et al., 2020; Du et al., 2013). However, the relationship between mixing layer structure and $PM_{2.5}$ concentration depends on the site, observation period, and the properties of MLH retrievals (Geiß et al., 2017; Lu et al., 2019). Even though the link between $PM_{2.5}$ concentrations and MLH has been investigated in many studies, most observations were conducted in winter conditions and few studies in hot seasons. Interestingly, in some cities, such as Delhi (Murthy et al., 2020) and Shanghai (Pan et al., 2019; Miao et al., 2021), the increase in $PM_{2.5}$ has been observed when MLH increased during summertime. As for O_3, the relationship between the changes in the MLH and O_3 concentrations is very complex. Both increase or decrease of O_3 has been observed corresponded to the growth of MLH. First, O_3 concentration decreases along with the increase of MLH owing to dilution.

Second, an increase in MLH generally promotes the downward mixing of upper air containing higher O_3 (Ma et al., 2021; Haman et al., 2014; Xu et al., 2018). In addition, the meteorological conditions along with the changes of MLH can influence O_3 concentrations through effecting O_3 gaseous precursors or production rates (Porter and Heald, 2019; Zhang et al., 2022). The combined effects of these processes ultimately determine whether O_3 decreases or increases.

Other meteorological variables in the mixing layer were also found to significantly affect $PM_{2.5}$ and O_3 concentrations. The poor air quality in the NCP was tightly associated with near-surface southerly winds and warm stagnant conditions during summertime (Zhang et al., 2015a). The increase in $PM_{2.5}$ concentration often coincided with high relative humidity (RH) conditions (Liu et al., 2017b), which was beneficial to liquid-phase heterogeneous reactions and fine particle hygroscopic growth (Seinfeld and Pandis, 2006; Wang et al., 2016; Zhang et al., 2015b). Temperature was essential to secondary chemical reaction (Dawson et al., 2007). The increase in temperature can promote chemical reaction rates, but also stimulate the evaporation of semi-volatile aerosol components, such as nitrate (Wen et al., 2018). For O_3, elevated O_3 concentrations generally happened on days with strong sunlight and low wind speeds, which favored the photochemical production and the accumulation of O_3 and its precursors. Several studies have shown that O_3 was significantly positive correlated with temperature, but negatively correlated with RH (Li et al., 2021; Hou and Wu, 2016; Steiner et al., 2010).

Long-term $PM_{2.5}$ composition measurements in the NCP showed an increase in the contributions of secondary species, e.g., sulfate (SO_4^{2-}), nitrate (NO_3^-), ammonium (NH_4^+), and organic matter (OM), to total $PM_{2.5}$ in recent years (Cheng et al., 2019; Wang et al., 2022b). As air quality improved ($PM_{2.5}$< 50 $\mu g\ m^{-3}$), the correlation between O_3 and $PM_{2.5}$ tended to change from negative to positive in China (Chu et al., 2020). One speculative reason for this phenomenon is that $PM_{2.5}$ does not reduce actinic flux and HO_2 radical significantly when the $PM_{2.5}$ concentration was low. On the other hand, $PM_{2.5}$ and O_3 tend to be positively correlated possibly due to their common precursors, such as VOCs and NOx, and their simultaneous generation in photochemical reactions. In addition, the generation of O_3 would cause the enhancement of atmospheric oxidation capacity, and catalyze the generation of the secondary $PM_{2.5}$ (Cheng et al., 2019; Kang et al., 2021; Wu et al., 2022). Even though some studies have discussed the correlations between MLH and some secondary pollutants, the understanding of the interaction between O_3 and $PM_{2.5}$ (including its major components) along with the evolution of mixing layer during warm seasons remained poor owing to the limited observations of $PM_{2.5}$ chemical species

involved. The regional-scale observation can represent the variation characteristics for this area and avoid the spatial heterogeneity between the sites. However, to the best of our knowledge, previous observational studies were mostly limited to specific cities. Therefore, it's encouraged to analyze multiple data sources to determine overall trends rather than making conclusions based on a single dataset.

According to the hourly concentrations of $PM_{2.5}$ and MDA8 O_3 in China over the years of 2013–2020, the months of June and July can well represent the typical characteristics of O_3–$PM_{2.5}$ coordinated pollution during warm seasons in the North China Plain (NCP) (Dai et al., 2023). To enhance the understanding of the linkages between mixing layer structure and air pollution, in this study, a regional-scale field observation of meteorological factors, O_3, $PM_{2.5}$ concentration and its secondary composition were conducted in the NCP from June 1 to July 31, 2021. For the first time, the potential association among ground-level observed O_3, $PM_{2.5}$ and its dominant components, and mixing layer meteorological conditions will be explored in the NCP during summertime.

2 Data and methods

2.1 Measurements

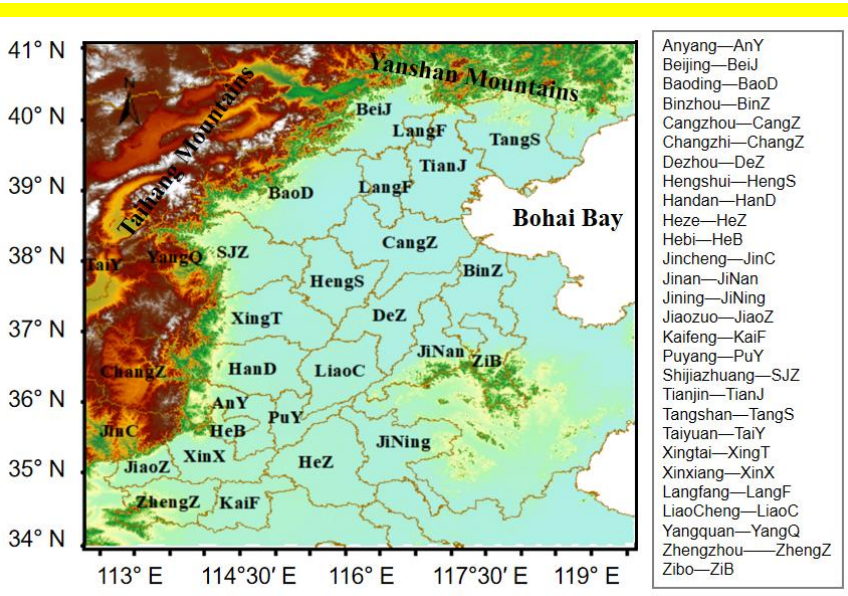

Figure 1. Location of monitoring stations in the NCP.

In this study, observation was made in the North China Plain (NCP) from June 1 to July 31, 2021. The air pollution observation stations in the NCP covered two megacities (BeiJ and TianJ) and 26

surrounding cities. The geographic locations of these stations are marked in Figure 1. The North China Plain (NCP) is surrounded to the west by the Taihang Mountains, to the north by the Yan Mountains, and to the east by the Bohai Sea. The hourly concentrations of ground-level O_3, $PM_{2.5}$ and its major components (SO_4^{2-}, NO_3^-, NH_4^+, and OC), and meteorological variables, including air temperature, relative humidity (RH), wind speed (WS) and direction (WD), and 24-h accumulated precipitation, at the sites were obtained from the platform of National Atmospheric Particulate Chemical-Speciation-Network, which is established for improving the understanding of the heavy pollution formation mechanism in the NCP and supporting the decision-making of local governments and state administration. Hourly SO_2, NO_2, O_3, $PM_{2.5}$ and its chemical compositions were recorded at the $PM_{2.5}$ component network, which was selected followed the Technical Regulation for Selection of Ambient Air Quality Monitoring Station published by the Ministry of Ecology and Environment of the People's Republic of China (HJ664−2013). The monitoring sites of $PM_{2.5}$ component network were mostly set up within the cities, and can reflect the average pollution level of each city. Details for the near-ground observation stations of $PM_{2.5}$ component network were shown in Table S1. Mass concentrations of SO_4^{2-}, NO_3^-, and NH_4^+ in $PM_{2.5}$ were continuously measured at a 1-h resolution by MARGA (model ADI 2080) or AIM-IC (URG 9000D) equipped with a $PM_{2.5}$ sampling inlet. These two IC-based online instruments have shown good performance through instrument intercomparison studies or comparison to offline filters under clean to moderately polluted conditions (Markovic et al., 2012; Wu and Wang, 2007; Park et al., 2013; Rumsey et al., 2014). Organic carbon (OC) was measured online by Sunset Semi-Continuous Carbon Analyzer (Sunset Laboratory Inc, USA). The concentration of OM can be obtained by multiplying the OC concentration by a factor of 1.6 (Li et al., 2021). $PM_{2.5}$, O_3, NO_2 and SO_2, were recorded hourly based on Thermo Scientific samplers and analyzers. Detailed descriptions of these online sampling instruments can be found in our previous works (Kong et al., 2018; Liu et al., 2017a; Pang et al., 2020; Wang et al., 2022b). The meteorological variables were recorded in the national meteorological observation stations, and the information of each station can be obtained from the public website of China Meteorological Administration (http://data.cma.cn/data/cdcindex/cid/0b9164954813c573.html). The temporal resolution of air temperature, RH, WS and WD was 1-h. To avoid the influence of diurnal boundary layer cycles, in this article we focused on the relationships between daily mean air pollutants and meteorological factors. The daily mean meteorological factors, $PM_{2.5}$ and its major secondary components were calculated

from the hourly data; daily O_3 concentration was characterized by the maximum daily 8 h average ozone (MDA8 O_3). Details for the near-ground observation species and the metrics were shown in Table S2.

To better demonstrate the overall change characteristics of regional air pollution and meteorological conditions during the observation period, the occurrence frequency (%), which means the proportion of the number of cities at each air pollutant or methodology level, was calculated based on the following equation:

$$\text{Occurrence frequency}_{X}^{level} = \frac{N_{X}^{level}}{\text{Total } N_X} \times 100\ \% \quad (1)$$

where X means the air pollutants or methodology factors, N_{X}^{level} represents the number of cities at each X level, $\text{Total } N_X$ represents the total number of cities.

2.2 The calculation of mixing layer heights

In recent years, many works have progressed in the atmospheric boundary layer characteristics, and analyzed the impacts of these parameter on air pollution. Planetary boundary layer (PBL), as one of the critical parameters to air quality modeling, has been well explored. However, PBL usually refers to the large-scale Ekman dynamic boundary layer (Haugen et al., 1971; Wang et al., 2014; Zhang et al., 2005). The way with which boundary layer describes the influences of air pollution is easily duplicated and confused (Niu et al., 2017). It is unreasonable to some extent, if the characteristic of the air pollution related to near-surface boundary layer is evaluated by using the concept of PBL. For air pollution measurement, one of selected functionalities of parameterization scheme for pollution mixing layer is to judge whether an air mass over a specific locality satisfies the “static and stable” attribute or not. Therefore, in this work, to express the basic physics for diagnosing meteorological conditions, we used the concept of pollution mixing layer height (MLH) proposed by Wang et al. (2017), which was based on the classical synoptic theory according to the level of convective condensation layer, and the details of this method can be seen in previous work (Wang and Yang, 2000; Wang et al., 2017).

To be specific, we define the height close to the cloud base as the height of super-saturation layer (H_SSL), and the isoentropic atmospheric process meets the level of convective condensation layer (LCL) in the super-saturation state, i.e., it is very close to the H_SSL. Iterative algorithm is used to work out the H_SSL (Wang and Yang, 2000):

$$H\_SSL \approx LCL = 6.11 \times 10^2 \times \left(\frac{0.622+0.622\frac{e_s}{p-e_s}}{0.622\frac{e_s}{p-e_s}}\right), \quad (2)$$

$$e_s = 6.22 \times \exp\frac{17.13(T-273.16)}{T-38}, \quad (3)$$

where e_s represents saturated water vapor pressure, T is temperature (K). Eq. (2) can be used to calculate the H_SSL which is favorable for pollutant mixing and represented by (P). Below this height, the atmosphere gets supersaturated, causing the pollution mixing and wetting process in the low altitude to continue, so this height is called the height of pollution mixing layer (MLH). Thus, MLH can be derived in the following expression:

$$MLH \approx H\_SSL \approx LCL = 6.11 \times 10^2 \times \left(\frac{0.622+0.622\frac{e_s}{p-e_s}}{0.622\frac{e_s}{p-e_s}}\right), \quad (4)$$

According to the relationship between air pressure and height, the units of MLH can be converted to the height expression in meters:

$$\int_{p_0}^{p_z} dp = -\int_0^z \rho_0 g dz, \quad (5)$$

where z is the height, ρ_0 is the density of gas, p_z and p_0 represent the air pressure in the height of z and 0, respectively.

Several works have verified the reliability of the results based on this method. With this method, Wang et al. (2017) well characterized the features of mixing layer height in highly-sensitive areas of pollution in China. Wang et al. (2022c) also used this method to explore the $PM_{2.5}$ and O_3 superposition-composite pollution event during spring 2020 in Beijing, China, and the hourly evolution of MLH, O_3, and $PM_{2.5}$ during the observation period were analyzed. In addition, Niu et al. (2017) has applied this method in Beijing, and the results showed that the pollution mixing layer can well present the change characteristics of haze pollution process. In this work, we further clarified the concept of MLH, and applied this method to investigate the impacts of MLH upon the change characteristics of ozone and fine particulate matter.

3 Results and discussions

3.1 General characteristics

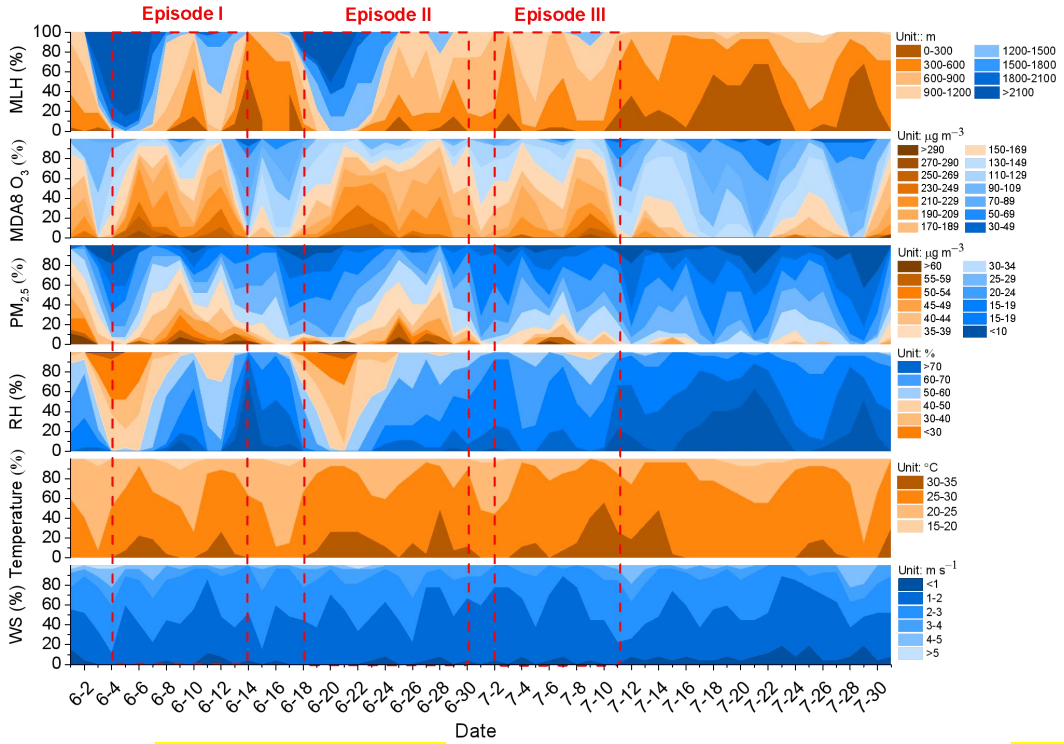

Figure 2. The occurrence frequency (%) of $PM_{2.5}$, MAD8 O_3, and meteorological factors under different levels in the NCP from June 1 to July 31, 2021. The color shading represents different categories classified by $PM_{2.5}$, MDA8 O_3, and meteorological factors. The red dash boxes represent three typical $PM_{2.5}$ and O_3 co-polluted episodes: June 4–14 (Episode I), June 18–29 (Episode II), and July 2–11 (Episode III), 2021.

The summertime change characteristics of ground-level meteorological factors (MLH, RH, temperature, and WS), MDA8 O_3, $PM_{2.5}$ and its major components in the NCP were demonstrated in Figure 2 and Figure S1. The primary atmospheric pollutant in the NCP during the summertime was O_3, and the concentrations of MDA8 O_3 averaged over all sites in the NCP varied from 74.94 μg m^{-3} to 219.28 μg m^{-3}, with the mean value of 151.72 μg m^{-3} (Table 1). The O_3 pollution lasted nearly the whole observation period, characterized by frequent and long-lasting pollution episodes. The $PM_{2.5}$ concentration was much lower comparing with ozone, with the mean, maximum, and minimum of the regional daily mean $PM_{2.5}$ concentration as 25.62 μg m^{-3}, 45.62 μg m^{-3}, and 11.32 μg m^{-3}, respectively, during the observation period. NO_3^- was the prominent $PM_{2.5}$ component, with the mean concentration of 7.76 μg m^{-3}. According to the National Ambient Air Quality Standard of China (GB3095-2012), the daily $PM_{2.5}$ averages in "2+26" cities can meet the Level II standard of 75 μg m^{-3}, while exceeding the level I standard (35 μg m^{-3}). As showed in Figure 2, regional $PM_{2.5}$ pollution processes corresponded well with the increasing processes of MDA8 O_3. Here, we define a O_3–$PM_{2.5}$ co-polluted episode as a

set of continuous days (longer than 4 days) with MDA8 O_3 and daily mean $PM_{2.5}$ (in more than 10 % NCP cities) exceeding 160 μg m^{-3} and 35 μg m^{-3}, respectively. According to this criterion, three typical O_3–$PM_{2.5}$ co-polluted episodes were selected: June 4–14 (Episode I), June 18–29 (Episode II), and July 2–11 (Episode III), 2021.

During these three typical episodes, the synchronous change characteristics of air pollutants and mixing layer meteorology were analyzed. In Episode I and II, when MLH higher than 2100 m, both MDA8 O_3 and $PM_{2.5}$ concentrations were low. Along with the reduction of MLH (from 1800–2100 m to 1200–1800 m), regional MDA8 O_3 and $PM_{2.5}$ concentration both gradually climbed up. When MLH fell in the range of 1200–1800 m, MDA8 O_3 concentration reached the maximum with about 80 % areas higher than 170 μg m^{-3}. We found that there is a lag time between the concentration peak of MDA8 O_3 and that of $PM_{2.5}$ along with the reduction of MLH. With the further decrease of MLH, MDA8 O_3 turned to decline, while $PM_{2.5}$ kept stable or continued to increase when regional MLH in the range of 600–1200 m. In Episode III, the MLH in most cities was lower than 1200 m, and the regional MDA8 O_3 and $PM_{2.5}$ pollution conditions were lighter than other episodes, with 80 % $PM_{2.5}$ values lower than 35 μg m^{-3}. It's interesting to note that the change characteristics of SO_4^{2-} and NO_3^- were different (Figure S1), and the regional peaks of these two components were inconsistent, especially in Episode II. With the evolution of MLH, NO_3^- climbed up and peaked on June 24 when regional MLH lower that 900 m, while SO_4^{2-} reached the maximum on June 28 when MLH was around 900–1500 m. This may be related to other synchronized mixing layer meteorology factors, such as RH and temperature. For example, the evolution of mixing layer often accompanied with changes in temperature. The increase in temperature can promote the chemical formation rate of these secondary components, but also stimulate the volatilization of NO_3^- to gaseous state (HNO_3) and lead to the decrease in NO_3^- concentration. Further analysis about the response of O_3, $PM_{2.5}$ and its secondary components to different mixing layer meteorology factors will be conducted in the following sections.

Table 1. General information on O_3–$PM_{2.5}$ co-polluted episodes from June 1 to July 31, 2021.

	Episode I			Episode II			Episode III			Summer		
	Ave.	Min	Max	Ave.	Min	Max	Ave.	Min	Max	Ave.	Min	Max
Gaseous pollutants (μg m^{-3})												
MDA8 O_3	170.80	85.62	219.28	180.65	142.10	204.15	168.70	111.79	199.39	151.72	74.94	219.28
SO_2	10.01	6.48	14.44	9.09	6.11	12.48	6.75	5.72	8.00	7.59	4.79	14.44

NO_2	24.61	16.26	31.81	22.89	14.11	32.15	17.66	13.12	21.00	19.31	10.90	32.15
$PM_{2.5}$ and its major components (μg m^{-3})												
$PM_{2.5}$	30.55	15.74	42.67	28.33	17.22	42.52	25.05	20.84	31.75	25.62	11.32	45.62
NO_3^-	8.74	2.16	16.44	8.29	2.85	18.00	7.67	5.87	13.44	7.76	2.16	18.24
SO_4^{2-}	7.22	2.81	10.25	7.32	4.02	12.15	7.12	5.48	8.92	7.04	2.81	12.15
NH_4^+	5.51	1.42	9.34	5.52	2.27	9.29	5.38	4.46	8.21	5.30	1.42	9.88
OC	5.11	2.74	6.60	4.71	3.25	6.75	4.11	2.90	5.30	4.32	2.69	6.75
Meteorological variables												
MLH (m)	1342.73	305.93	2423.42	1190.36	626.51	2127.31	740.86	460.91	950.10	855.99	305.93	2423.42
T (°C)	26.24	23.86	28.91	27.41	25.53	28.76	27.58	24.85	30.14	26.69	22.48	30.14
RH (%)	57.01	32.78	90.54	56.90	37.04	70.60	71.45	64.64	80.38	68.70	32.78	90.54

3.2 Evolution of ozone with mixing layer meteorology

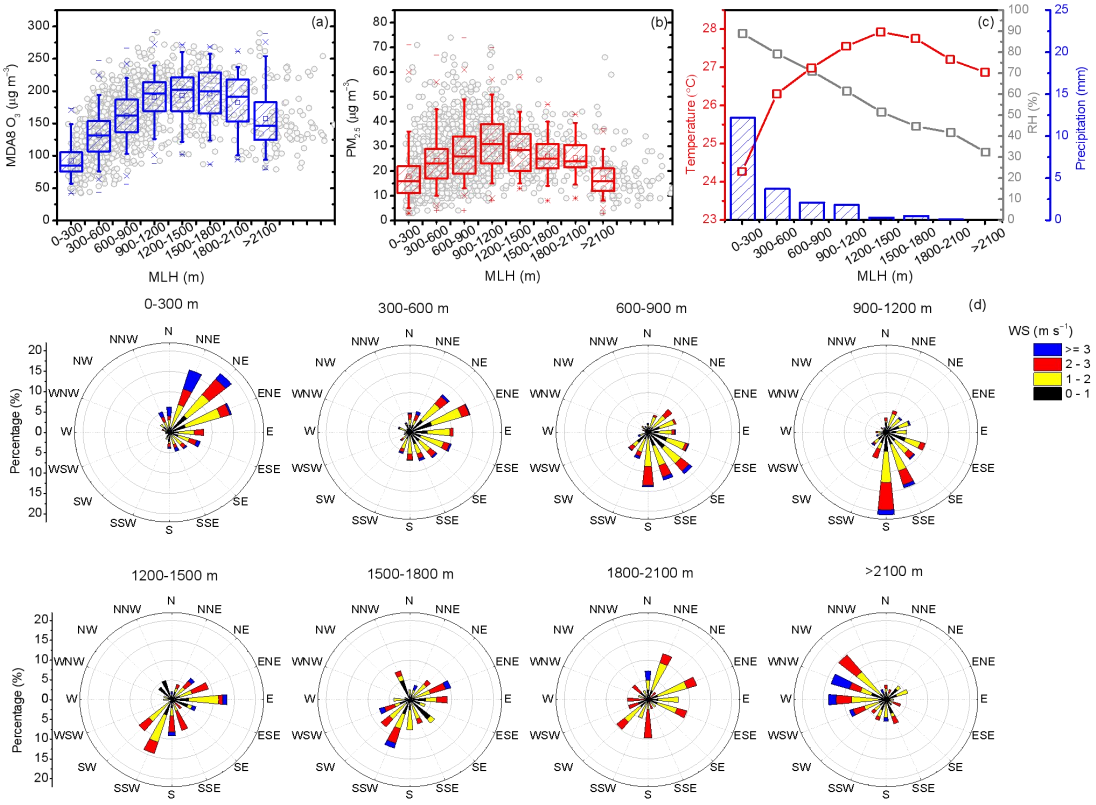

Figure 3. The variation characteristics of (a) MDA8 O_3, (b) $PM_{2.5}$, (c) temperature, RH, 24-h precipitation, and (d) WS and WD in different MLH conditions. Box plots in (a) and (b) show the inter quartile range (the distance between the bottom and the top of the box), median (the band inside the box), and 95 % confidence interval (whiskers above and below the box) of the data. S: south; N: north; E: east; W: west.

To quantify the effect of MLH on near-ground O_3 concentrations, relationships between MLH and

MDA8 O_3 were analyzed (Figure 3a). Here we used a data binning method to remove the expected day-to-day atmospheric variability from sampling uncertainty (Dian et al., 2010), which has been applied elsewhere (Lou et al., 2019). The MLH was grouped into 8 classes with 300 m width: 0–300, 300–600, 600–900, 900–1200, 1200–1500, 1500–1800, 1800–2100 and > 2100 m. It was found that MDA8 O_3 concentration dramatically increased when MLH in the range of 0–900 m, and leveled off when MLH at around 900–1800 m, with the maximum MDA8 O_3 of 195.88±42.76 μg m^{-3}, then turned to decrease with further development of MLH. This nonlinear relationship between MDA8 O_3 and MLH was is consistent with the results conducted by Zhao et al. (2019) and Reddy et al. (2012). The work by Zhao et al. (2019) found that O_3 concentration was the highest at medium boundary layer heights (1200–1500 m) in Shijiazhuang, China. In India, days of higher O_3 concentrations were also associated with higher boundary layer height (Reddy et al., 2012).

This relationship observed between MDA8 O_3 and MLH is very complex. Previous works have shown that higher height of mixing layer can lead to the mixing of near surface air with the O_3 rich air aloft, resulting in the observed enhancements in surface O_3 concentration (Reddy et al., 2012). Concurrently, the evolution of mixing layer were strongly associated with the change of other meteorological conditions, such as air temperature, RH and precipitation, which can also affect O_3 concentration (Haman et al., 2014). The combined effects of these processes ultimately determine whether ground-level O_3 increases or not along the evolution of mixing layer. The increase of MLH often coincided with higher air temperature, lower RH, and less precipitation (Figure 3c), which were more conducive to O_3 production (Ma et al., 2021; Xu et al., 2018). As shown in Figure 4a–c, as MLH kept constant, MDA8 O_3 concentration climbed up with increase in temperature but decrease in RH and precipitation levels. Possible reasons for these results could be: (1) the increase in RH can contribute to the depletion of O_3, and lead to weakened O_3 related photochemical reaction (Ma et al., 2021; Yu, 2019); (2) due to higher RH or rain fall, gaseous precursors and O_3 can be washed out from the atmosphere trough wet deposition (Reddy et al., 2012); and (3) the rise of temperature can accelerate the emission rate of gaseous precursors, such as biogenic VOCs and soil NO_X (Dang et al., 2021; Porter and Heald, 2019), and also stimulate the photochemical reaction rate in the generation of O_3 (Ma et al., 2021). Besides, wind fields could alter surface O_3 concentrations by transporting O_3 or its

precursors in and out of this region (Ma et al., 2021). As shown in Figure S2, during the whole campaign, the NCP was dominated by winds from northeast and south (45−225°). Because more than 75 % WD were in the rang of 45−225°, the WD was classified into 4 categories: 45−90, 90−135, 135−180, and 180−225°. As shown in Figure 3d, along with the evolution of mixing layer, the WD gradually changed from northeast (MLH=0−600 m) to southeast (MLH=600−900 m) and south (MLH=900−1200 m). The southerly wind can transport the gaseous pollutants or O_3 from the southern part of the plain area to the northern part, and the Taihang mountains may block pollutant transport, leading to the accumulation of pollutants along the foot of the Taihang Mountains. It's noted that the concentration of MDA8 O_3 was higher when the plain dominated by southerlies (180−225°) when MLH lower than 1200 m (Figure 4e). In general, WS could affect the diffusion of air pollutants. Due to the limited dilution and dispersion effect of weak wind, the MDA8 O_3 concentrations at low wind speed (0−1 m s^{-1}) were relative higher than other WS conditions (Figure 4d) .

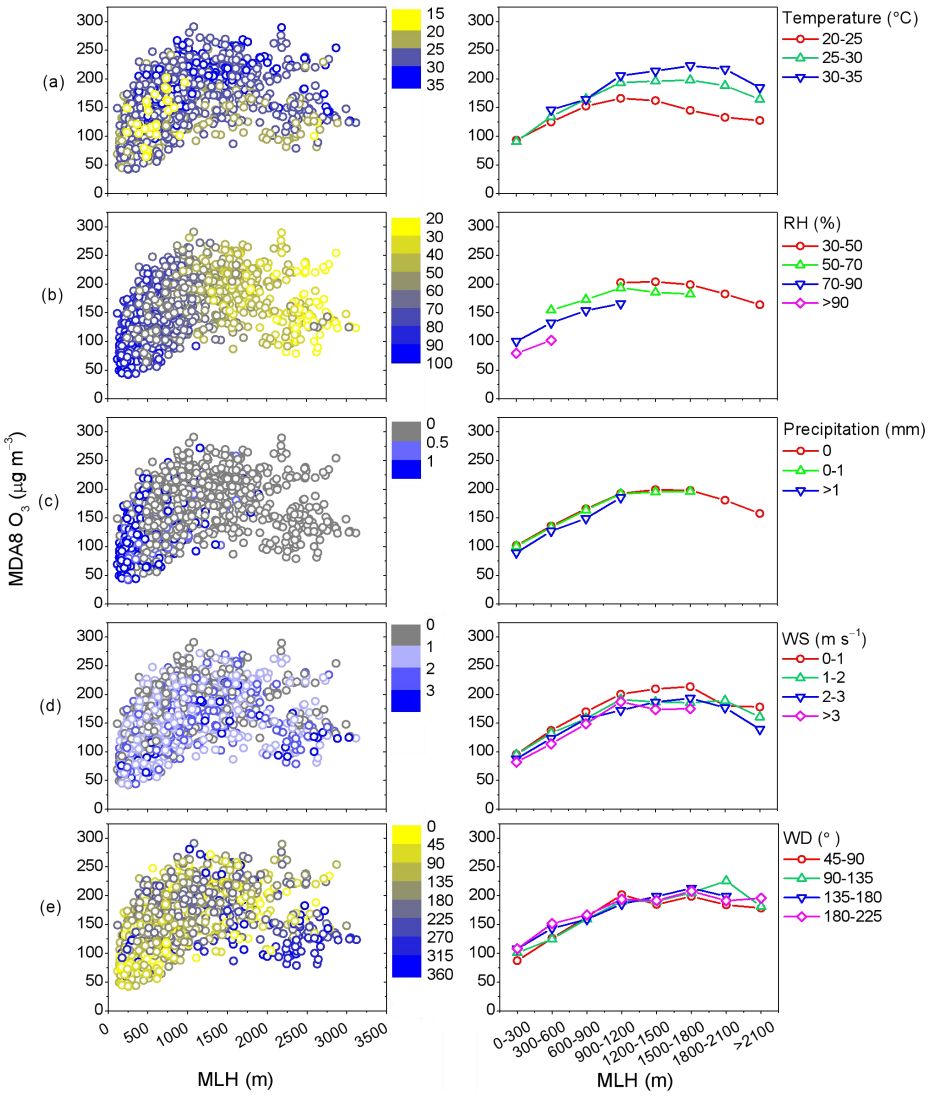

Figure 4. The distribution characteristics of the MDA8 O_3 concentrations with the evolution of MLH under different (a) temperature, (b) RH, (c) precipitation, (d) WS, and (e) WD conditions.

3.3 Evolution of $PM_{2.5}$ and its secondary compositions with mixing layer meteorology

The concentration distribution of surface $PM_{2.5}$ in different MLH bins has been shown in Figure 3b. Interestingly, $PM_{2.5}$ showed similar change profile as MDA8 O_3, which initially increased and then declined along with the growth of MLH. $PM_{2.5}$ concentration reached the maximum of 31.65 μg m^{-3} when MLH fell in the range of 900–1200 m, and the concentration has increased by 1.51 μg m^{-3} through the rise phase for the variation of 100 m MLH. This phenomenon was quite different with the results in cold seasons (Pan et al., 2019; Du et al., 2013; Murthy et al., 2020). It has been suggested that the narrowing of mixing layer will compress air pollutants into a shallow layer, resulting in elevated pollution levels, thus MLH has been illustrated as the key factor to aggravate the haze events in large cities of China in winter. However, the response of $PM_{2.5}$ concentration to MLH is not only determined by the vertical stratification of the mixing layer, but also by local sources, secondary chemical formation, wet deposition, and the wind field (Lu et al., 2019; Geiß et al., 2017; Pan et al., 2019; Miao et al., 2021; Lou et al., 2019). Noted that in this work there were still some extreme high $PM_{2.5}$ values under low MLH condition as shown in Figure 3b, and this phenomenon will be discussed in the following part when exploring the effect of precipitation.

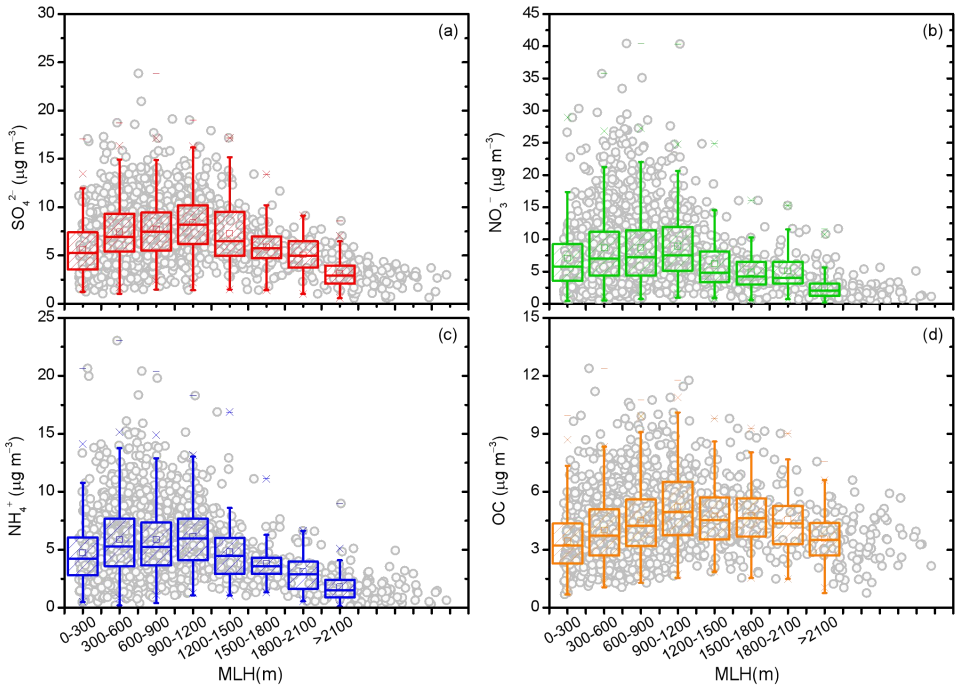

Figure 5. The variation characteristics of (a) SO_4^{2-}, (b) NO_3^-, (c) NH_4^+, and (d) OC in different MLH

conditions. Box plots show the inter quartile range (the distance between the bottom and the top of the box), median (the band inside the box), and 95 % confidence interval (whiskers above and below the box) of the data.

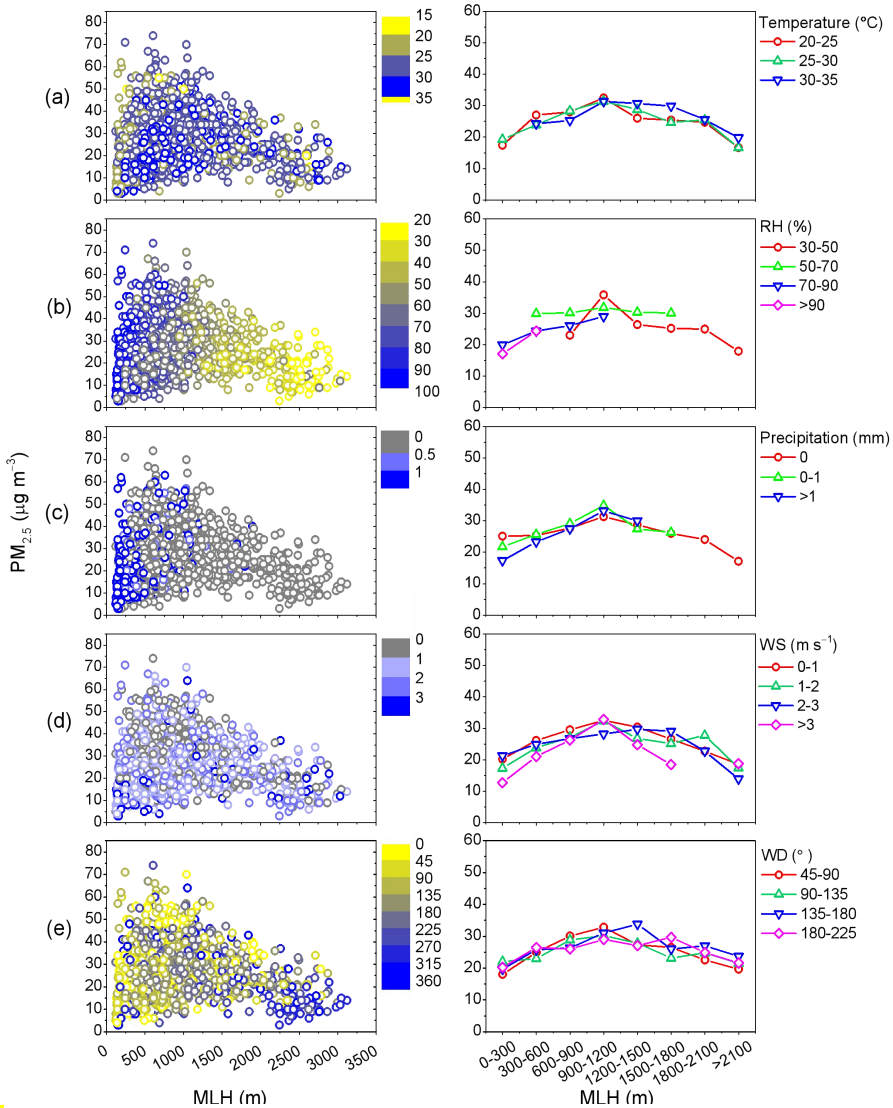

Figure 6. The distribution characteristics of the $PM_{2.5}$ concentrations with the evolution of MLH under different (a) temperature, (b) RH, (c) precipitation, (d) WS, and (e) WD conditions.

The response of $PM_{2.5}$ concentrations to mixing layer structure was the net effect of the changes in $PM_{2.5}$ major chemical components, such as SO_4^{2-}, NO_3^-, NH_4^+, and OC. Figure 5 showed the changes in the major $PM_{2.5}$ components due to the evolution of mixing layer. All the secondary components showed increasing trends when MLH lower than 1200 m, with SO_4^{2-} and OC showing the highest increment, followed by NO_3^- and NH_4^+. When MLH changed from 300−600 m to 900−1200 m, the increment was not significant for NO_3^- and NH_4^+. As NH_3 was generally abundantly supplied in the NCP, the formation of NH_4^+ was dominantly controlled by the reaction of ammonia with sulfate and

nitrate aerosols, and the changes in NH_4^+ were a consequence of the changes in SO_4^{2-} and NO_3^- (Chow et al., 2022). When MLH<1200 m, the mass fraction of NO_3^- was higher than SO_4^{2-} in $PM_{2.5}$ (Figure S3), and the change characteristics of NH_4^+ along with the evolution of mixing layer were consistent with that of NO_3^-. The mass ratio of SO_4^{2-} to NO_3^- gradually increased along with the development of mixing layer. When MLH higher than 1200m, SO_4^{2-} surpassed NO_3^- and became the dominant $PM_{2.5}$ component. The difference in the relationships between these aerosol species and MLH reflected the intrinsic complexity mechanisms of $PM_{2.5}$ formation, which were probably related to other meteorological parameters, such as temperature, RH, precipitation, WS, and WD. In order to understand how the other meteorological factors impacted the relationship between MLH and $PM_{2.5}$, we demonstrated the statistics on the concentration distribution of $PM_{2.5}$ and its dominant components with the increase of MLH under different RH, temperature, precipitation, WS, and WD conditions in Figure 6 and Figure 7.

Temperature is not only essential to the secondary chemical reaction of trace gases, but also the gas–particle partitioning of volatile $PM_{2.5}$ species. The response of $PM_{2.5}$ and its dominant components to MLH followed similar change characteristics under different temperature conditions, all increasing with the development of mixing layer when MLH lower than 1200m. The response of $PM_{2.5}$ to temperature was largely the result of opposite changes in NO_3^- and SO_4^{2-} concentrations with a smaller role played by organics (Figure 7). Specifically, as MLH kept constant, SO_4^{2-} concentration climbed up with increasing temperature level, while the concentration of NO_3^- declined when temperature kept going up. Higher temperature may promote faster oxidation of SO_2 to SO_4^{2-}, resulting in a significant increase in SO_4^{2-} concentrations. Unlike SO_4^{2-}, which predominantly exists in the particle phase, NO_3^- could be either presented as nitric acid (HNO_3) in the gas phase or as ammonium nitrate (NH_4NO_3) in the particle phase (Chow et al., 2022). The temperature condition strongly influences the partitioning of nitrate between gas and particle phase. Higher temperature prompts the partitioning of nitrate to HNO_3, thus nitrate tends to exit in the gas phase, resulting in a significant decrease in NO_3^- and NH_4^+ concentrations.

The response of $PM_{2.5}$ and its dominant components to the evolution of mixing layer was more sensitive to RH, and distinct distribution characteristics under different RH ranges have been observed in Figure 6 (b) and Figure 7 (b). When MLH fell in the range of 300–900 m, the concentration of $PM_{2.5}$ (Figure 6b) and its major components (Figure 7b) mostly decreased with RH elevating from 50–70 %

to 70–90 %. Previous works have shown that when RH higher than 60%, local humidity-related physicochemical processes play important roles in transforming the gases to aerosols (Wang et al., 2022d; Liu et al., 2020). We considered that the RH range from 50% to 70% was more beneficial to the aqueous chemical production of major $PM_{2.5}$ components, then led to the increase of $PM_{2.5}$ concentration. It is worth noting that when MLH in the range of 0–300 m, with RH increasing from 70–90 % to > 90 %, the concentration of $PM_{2.5}$ (Figure 6b) and its major components (Figure 7b) severely dropped, which was probably related to the fast hygroscopic growth and enhanced wet deposition processes.

All aerosol species have wet deposition as a major sink, so precipitation is expected to have significant effects on $PM_{2.5}$ concentrations. As shown in Figure 6 (c), changes in the concentrations of $PM_{2.5}$ was sensitive to the rain events. When MLH fell in the range of 0–300 m, the concentration of $PM_{2.5}$ significantly decreased during rainfall period. Interestingly, when no rainfall occurred, even though $PM_{2.5}$ concentration kept stable under low MLH condition, the response of $PM_{2.5}$ concentrations to MLH still followed upward trend with MLH increasing from 300–600 to 900–1200 m. As for specific aerosol species (Figure 7c), NO_3^- and NH_4^+ concentration showed two obvious peaks, with one in the range of 0–300 m, and the other in 900–1200 m. Under low MLH condition, the concentrations of NO_3^- and NH_4^+ were high, with NO_3^- as the dominant species in $PM_{2.5}$ (Figure 8b). With the growth of MLH, NO_3^- and NH_4^+ initially decreased, but turned to increase again when MLH in the range of 900–1200 m. As for SO_4^{2-} and OC, the concentrations obviously increased with the elevation of MLH and has exceeded that of NO_3^- when MLH higher than 1200 m. As shown in Figure 8 (a), low mixing layer generally accompanied with cloudy and rainy conditions during summertime in the NCP in 2021, and only small fraction of days without rainfall has been captured during this period. Therefore, despite some high $PM_{2.5}$ or major aerosol species values have been witnessed under low MLH condition, the overall trend in Figure 3 (b) was still upwards along with the growth of mixing layer (MLH < 1200 m). The increase of $PM_{2.5}$ and its major chemical components under medium MLH condition was not only associated with the weaker particle removal process by precipitation, but also related to the enhancement of secondary aerosol formation due to appropriate chemical reaction environment.

WS can represent the atmospheric dissipation potential in the horizontal directions (Zhu et al., 2018). Low WS generally suggested weak pressure gradients and potentially a more favorable meteorological condition for $PM_{2.5}$ enhancement (Ma et al., 2021). As expected, the concentrations of

$PM_{2.5}$ (Figure 6d) and its aerosol species (Figure 7d) gradually decreased with the increase of WS. The response of these air pollutants to MLH followed similar upward trends under different WS conditions (MLH < 1200 m). Comparing with O_3, the impact of WD along with the increase of MLH seems different for $PM_{2.5}$ and its dominant components. When MLH in the range of 600−1200 m, the NCP was dominated by southeast or south wind (Figure 3d). However, when southeast or south wind prevailed, the corresponding $PM_{2.5}$ and its dominant components concentrations were comparable or even lower than other WD situations (Figure 6e and Figure 7e). This indicated that regional transport was not the dominant factor leading to the elevation of $PM_{2.5}$ and its aerosol species along with the evolution of mixing layer (MLH < 1200 m).

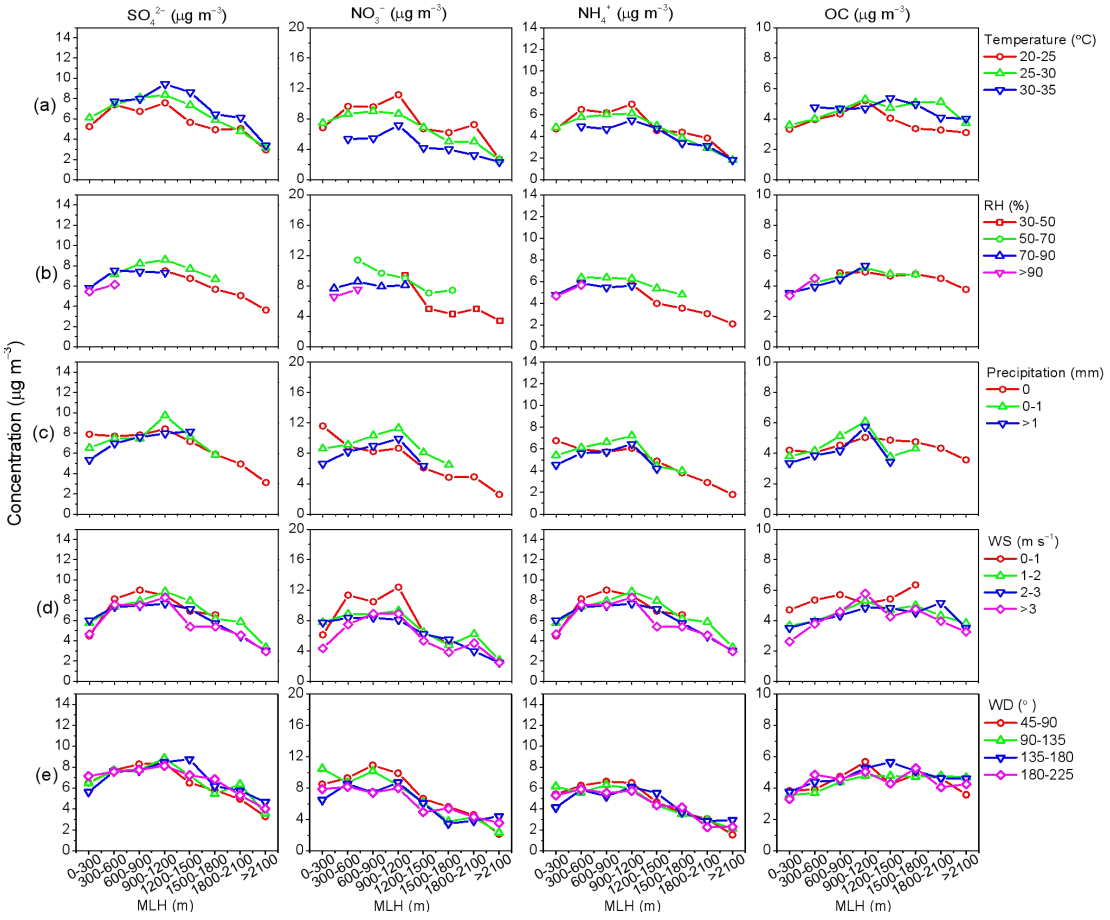

Figure 7. The distribution characteristics of NO_3^-, SO_4^{2-}, NH_4^+, and OC concentrations with the evolution of MLH under different (a) temperature, (b) RH, (c) precipitation, (d) WS, and (e) WD conditions.

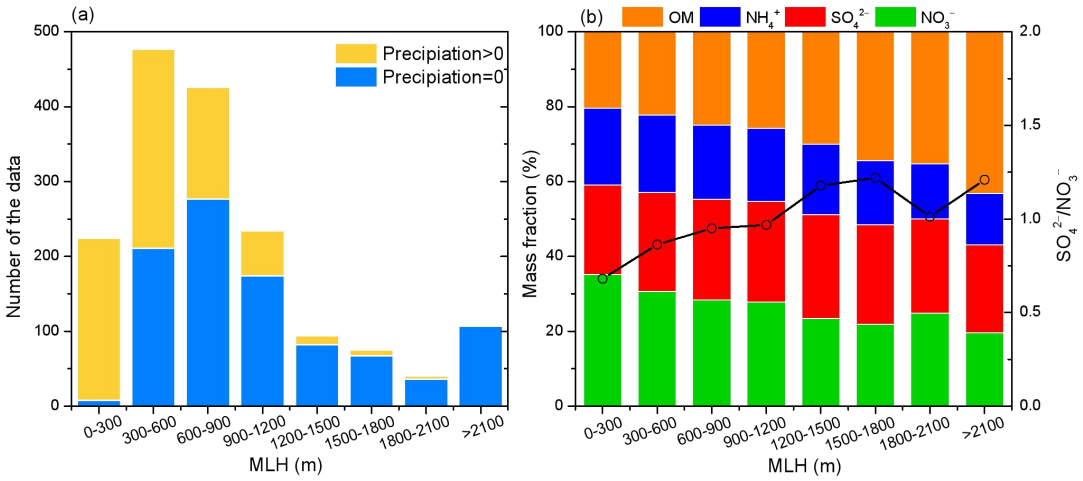

387

388 **Figure 8.** (a) The number distributions of the data when the daily precipitation larger than 0 mm or
389 equal to 0 mm along with the evolution of MLH. (b) The mass fractions of major $PM_{2.5}$ components
390 and the mass ratio of SO_4^{2-} to NO_3^- along with the evolution of MLH when the daily precipitation
391 equal to 0 mm.

392 **3.4 Superposition-composite effects of $PM_{2.5}$ and O_3 with the evolution of mixing layer**

393 **3.4.1 A case study of the typical $PM_{2.5}$-O_3 co-polluted episode**

394 Previous results indicated that MDA8 O_3 and $PM_{2.5}$ concentrations were closely related to the
395 evolution of BLH. The increasing trend of $PM_{2.5}$ concentration with the development of mixing layer
396 under medium MLH condition discussed before indicated that the evolution of mixing layer was not a
397 simple physical dilution process, and its influence on the enhanced secondary photochemical formation
398 should be considered as well. Figure 9 and 10 demonstrated a typical $PM_{2.5}$-O_3 co-polluted episode
399 (Episode II) during 18−29, 2021 to comprehensively present the relationship between the mixing layer
400 and pollutants. On June 18−20, MLH gradually increased from 600−1200 m to 1500−3000 m in the
401 southern and eastern part of the NCP, $PM_{2.5}$ and MDA8 O_3 concentrations concurrently increased and
402 showed similar spatial distributions. The wind speed dropped significantly on 20 June, and the value
403 was lower than 1 m s^{-1} in most cities. On 21−23 June, MLH started to decrease from 1500−3000 m to
404 1200−1800 m, $PM_{2.5}$ and MDA8 O_3 concentrations further increased, and the areas of high $PM_{2.5}$
405 concentrations also coincided well with those of MDA8 O_3 concentrations. During 24−25 June, MLH
406 continued to decrease, with some values even lower than 300 m. The MLH for the areas with high
407 MDA8 O_3 was in the range of 900−1500 m. Interestingly, the synchronized spatial change
408 characteristics of $PM_{2.5}$ and MDA8 O_3 were consistent when MLH in the range of 900−1200 m, while

inconsistent when MLH lower than 600 m. Significant rise of $PM_{2.5}$ concentration was observed in some cities with MLH lower than 300 m. It's noted that the dominant chemical composition of $PM_{2.5}$ in these areas was NO_3^-. On 28 June, the rise in MLH was observed in the central and the southern part in the NCP, and a surge of MDA8 O_3 and $PM_{2.5}$ concentrations both occurred, with 160−220 μg m^{-3} and 40−50 μg m^{-3} respectively. In general, most cities were dominated by weak winds from the east and southeast, which favored the formation of secondary pollutants from the gaseous precursors transported from the southeast part and promoted the accumulation of air pollutants.

To better understand this $PM_{2.5}$-O_3 co-polluted event, here we classified the observations during this typical event into four categories: O_3 polluted days (O_3PD; MDA8 O_3 concentration > 160 μg m^{-3} and $PM_{2.5}$ < 35 μg m^{-3}), $PM_{2.5}$ polluted days ($PM_{2.5}$PD; MDA8 O_3 concentration < 160 μg m^{-3} and $PM_{2.5}$ > 35 μg m^{-3}), O_3–$PM_{2.5}$ co-pollution days (O_3–$PM_{2.5}$CPD; MDA8 O_3 concentration > 160 μg m^{-3} and $PM_{2.5}$ > 35 μg m^{-3}), and non-polluted days (NPD; MDA8 O_3 < 80 μg m^{-3} and $PM_{2.5}$ < 35 μg m^{-3}). Figure 11 showed the meteorological and chemical characteristic of O_3–$PM_{2.5}$ CPD, O_3PD, $PM_{2.5}$ PD, and NPD. The results indicated that the values of MLH on O_3–$PM_{2.5}$CPD were between those on O_3PD and $PM_{2.5}$PD at around 900 m. On O_3–$PM_{2.5}$CPD, the oxidation ratio of sulfate (SOR, the molar ratio of sulfate to the sum of sulfate and SO_2) and oxidation ratio of nitrate (NOR, the molar ratio of nitrate to the sum of nitrate and NO_2) were the highest, with the values of 0.44 and 0.33, respectively, which indicated the strong secondary formation of SO_4^{2-} and NO_3^- promoted by high O_3 concentration. The $PM_{2.5}$PD occurred when MLH lower than 650 m, and the percentage of NO_3^- was the highest on $PM_{2.5}$PD. The rise of $PM_{2.5}$ in some cities under low MLH conditions may be attributed to three mechanisms. The first one is the accumulation effect due to unfavorable diffusion condition when MLH decreased. Second, these cities got little rain, and the effect of wet deposition was weak. In addition, the corresponding low T and high RH can stimulate the formation of NO_3^- from gaseous state (HNO_3). On O_3PD, the MLH was around 1300 m, and the NOR turned to decrease, demonstrating a more significant role of partitioning process between gas and aerosol than the atmospheric oxidation process under this stage. On NPD, the MLH was the highest, with the value of about 2400 m, and the $PM_{2.5}$ chemical composition was obviously dominated by OM.

To explore the relevance of hourly O_3, $PM_{2.5}$, its components and MLH, we have taken PuY and HeZ as examples. Figure S4 plotted the day-to-day variations along with the diurnal variations of O_3, $PM_{2.5}$, its components and MLH in PuY and HeZ during Episode II (June 18−29, 2021). The results

showed that there were large diurnal as well as day-to-day variability in the O_3 and $PM_{2.5}$ levels. The diurnal variations of MLH were clearly visible (Figure S5), with the rise in MLH during the daytime and the decrease in MLH at night. The concentration of $PM_{2.5}$ increased with the decrease of MLH at night, but the concentration of O_3 increased with the rise of MLH at daytime. Interestingly, we observed noontime soar of SO_4^{2-} and OC concentrations in PuY, and the values of SOR kept stable or even increase at noon. Besides, it's noted that O_3 and $PM_{2.5}$ both gradually accumulated with the development of mixing layer during June 18−21 and 26−28, which can be attributed to the O_3 and $PM_{2.5}$ superposition composite effects. The decrease in $PM_{2.5}$ at daytime with the rise of MLH can be offset partly by an increment in secondary pollutants formation derived from O_3 growth. Then with the decrease of MLH at night, the concentration of the original existing $PM_{2.5}$ increased due to unfavorable diffusion. In general, the conclusions in this work was only suitable to the day-to-day relationship between air pollutants and MLH. The hourly relationships were much more complicated and need more further analysis.

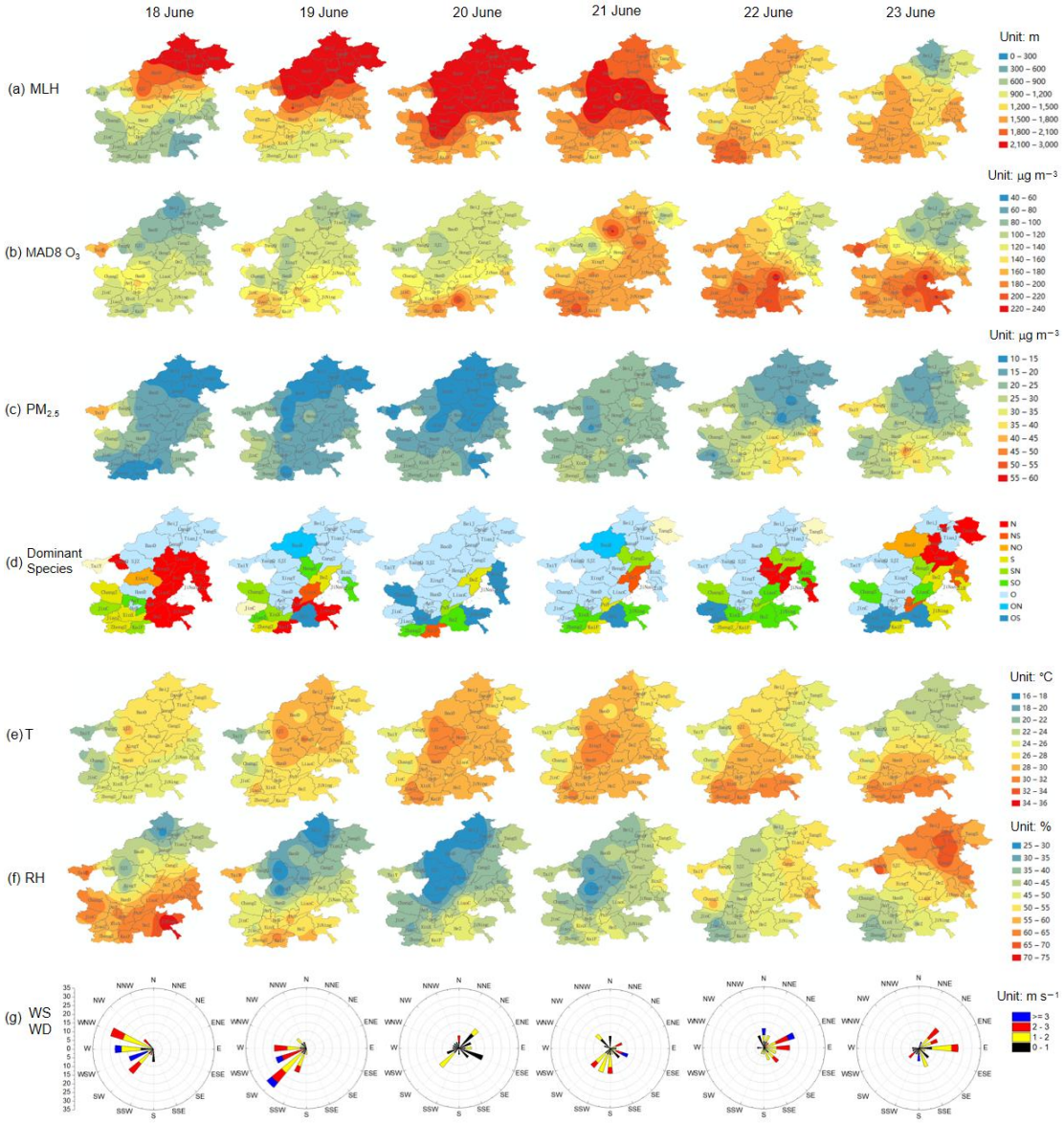

Figure 9. The spatial distribution of (a) MLH, (b) MDA8 O_3, (c) $PM_{2.5}$, (d) the dominant $PM_{2.5}$ chemical component (N: NO_3^- dominant, NS: NO_3^- and SO_4^{2-} dominant, NO: NO_3^- and OM dominant, S: SO_4^{2-} dominant, SN: SO_4^{2-} and NO_3^- dominant, SO: SO_4^{2-} and OM dominant, O: OM dominant, ON: OM and NO_3^- dominant, OS: OM and SO_4^{2-} dominant), (e) T, and (f) RH, (g) the overall change characteristics of WS and WD in the NCP from June 18 to 23, 2021. The dominant $PM_{2.5}$ chemical component type was identified as the method proposed by Wang et al. (2022b): if the mass fraction of the maximum component was 1.2 times higher than that of the secondary one, the former was considered as the dominant factor, otherwise both dominated $PM_{2.5}$ formation.

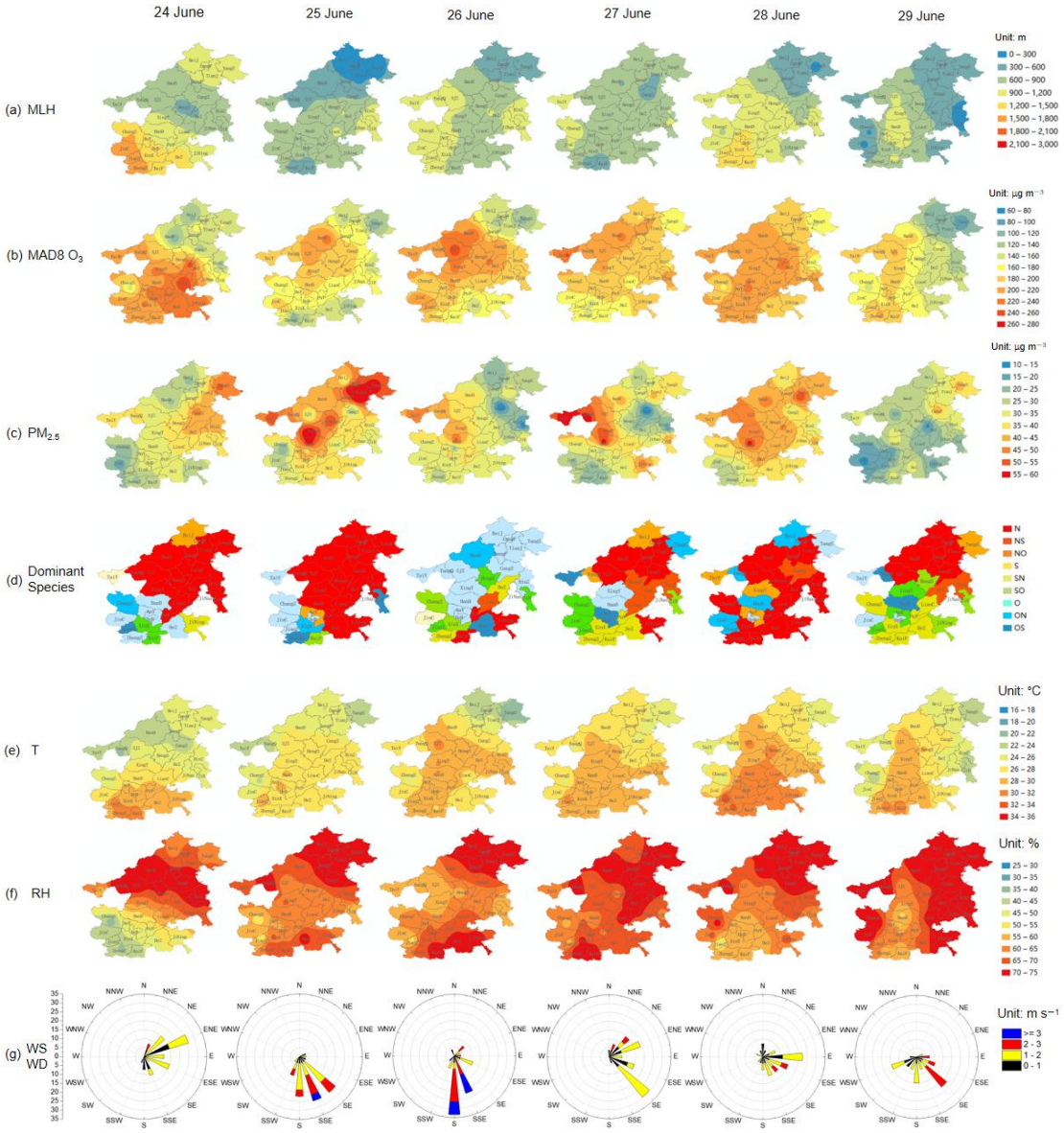

Figure 10. The spatial distribution of (a) MLH, (b) MDA8 O_3, (c) $PM_{2.5}$, (d) the dominant $PM_{2.5}$ chemical component (N: NO_3^- dominant, NS: NO_3^- and SO_4^{2-} dominant, NO: NO_3^- and OM dominant, S: SO_4^{2-} dominant, SN: SO_4^{2-} and NO_3^- dominant, SO: SO_4^{2-} and OM dominant, O: OM dominant, ON: OM and NO_3^- dominant, OS: OM and SO_4^{2-} dominant), (e) T, and (f) RH, (g) the overall change characteristics of WS and WD in the NCP from June 24 to 29, 2021. The dominant $PM_{2.5}$ chemical component type was identified as the method proposed by Wang et al. (2022b): if the mass fraction of the maximum component was 1.2 times higher than that of the secondary one, the former was considered as the dominant factor, otherwise both dominated $PM_{2.5}$ formation.

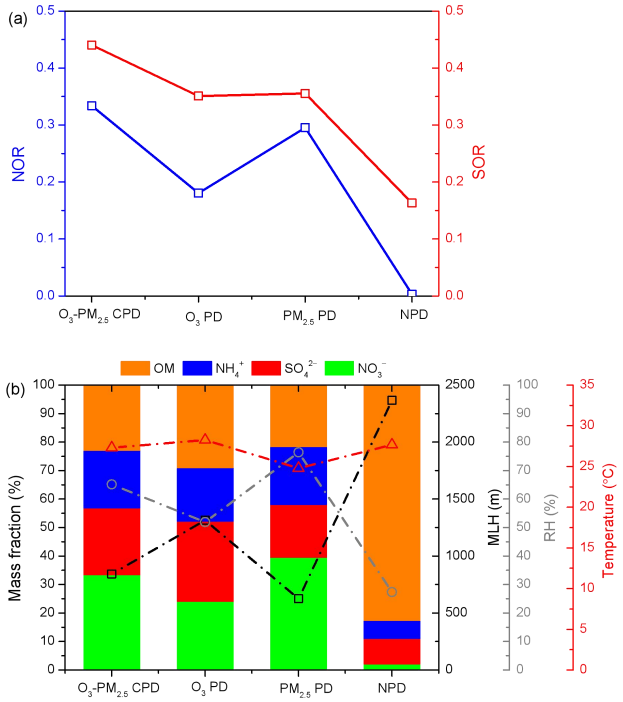

Figure 11. The distribution characteristics of (a) NOR and SOR, and (b) the mass fractions of major $PM_{2.5}$ components, MLH, RH, and temperature under O_3–$PM_{2.5}$ CPD, O_3 PD, $PM_{2.5}$ PD, and NPD conditions from June 24 to 29, 2021.

3.4.2 Interaction between $PM_{2.5}$ and O_3 along with the evolution of MLH

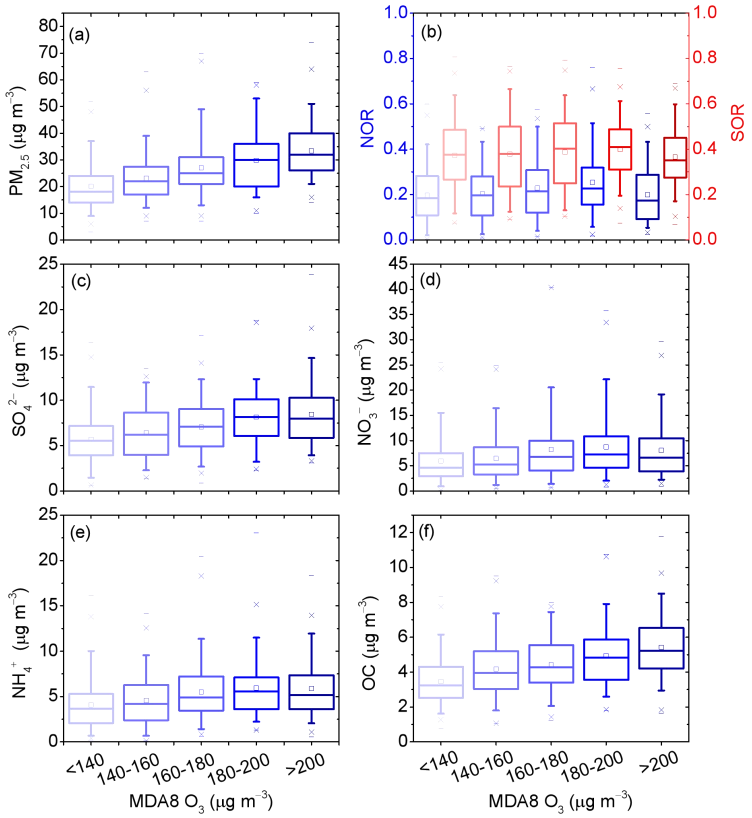

Figure 12. Box plots showing the statistics of (a) $PM_{2.5}$, (b) NOR and SOR, (c) SO_4^{2-}, (d) NO_3^-, (e) NH_4^+, and (f) OC for different MDA8 O_3 conditions (< 140 μg m^{-3}, 140–160 μg m^{-3}, 160–180 μg m^{-3}, 180–200 μg m^{-3}, > 200 μg m^{-3}). The distance between the bottom and the top of the box reflects the inter quartile range; the line and square in between are the median and mean values, respectively. The whiskers above and below the box refer the 95 % confidence interval of the data. Note that rainy days were excluded.

Figure 12 displays the box-and-whisker plots of $PM_{2.5}$ and its major components for different MDA8 O_3 conditions. To isolate the impacts of precipitation on $PM_{2.5}$ concentration, these rainy days when the daily rainfall amount greater than 0 mm were excluded in this section. Here the concentrations of $PM_{2.5}$ and its major components were found to increase synchronously with elevated MDA8 O_3 concentration, especially when MDA8 O_3 increased from < 140 to 180–200 μg m^{-3}.This summertime collaborative growth process of $PM_{2.5}$-O_3 has also been observed in other works (Wang et al., 2022a; Wu et al., 2022). With elevated MDA8 O_3 concentration, SOR and NOR both slightly increased, and reached the maximum when MDA8 O_3 at around 160–200 μg m^{-3}, which indicated the strong secondary formation of SO_4^{2-} and NO_3^- promoted by high O_3 concentration. When MDA8 O_3 increased from 180–200 to > 200 μg m^{-3}, the concentrations of NO_3^-, NH_4^+, and SO_4^{2-} kept stable or started to decrease, and the values of SOR and NOR decreased synchronously. During this stage, the high O_3 concentration often accompanied with dry and hot meteorological conditions, which was not beneficial to the aqueous chemical production and was conducive to the partitioning of nitrate to the gas phase.

To verify the potential impact of photochemical oxidation to the increase of $PM_{2.5}$ concentration with mixing layer development, the changes in $PM_{2.5}$ and MDA8 O_3 along with the increase of MLH were quantified in the "2+26" cities in the NCP. Linear regression equations between air pollutants and MLH were fitted during the initial increasing stage (300 < MLH < 1200 m) and their slopes were given in Figure 13. The slopes indicated the rates of the maximum changes in air pollutant concentration for a unit change in MLH (100 m). The slopes of $PM_{2.5}$ and O_3 were expressed as $\Delta PM_{2.5}$ and ΔO_3 (μg m^{-3} (100) m^{-1}). It was found that $\Delta PM_{2.5}$ was closely related to ΔO_3 (R^2=0.58), and obvious spatial difference in $\Delta PM_{2.5}$ and ΔO_3 was witnessed in the NCP during the observation period. $\Delta PM_{2.5}$ and ΔO_3 both showed high values in YangQ, , LangF and CangZ, with values of 7.56 and 20.24 μg m^{-3} (100) m^{-1} in YangQ, 5.75 and 18.97 μg m^{-3} (100) m^{-1} in LangF, and 4.02 and 19.49 μg m^{-3} (100) m^{-1} in

CangZ, respectively. Comparing with these cities, $\Delta PM_{2.5}$ and ΔO_3 were lowest in HeB, with the value of 3.54 and −2.02 μg m^{-3} (100) m^{-1}, respectively, which implied that the secondary formation here was weak and the surface $PM_{2.5}$ change characteristic was dominantly controlled by local emissions or vertical diffusion effect.

Comparing with winter, the photochemistry in summer is quite active due to the strong solar radiation. Even though deep MLH favors the dilution of air pollutants, higher MLH can also promote secondary chemical feedback through enhancing the availability of atmospheric oxidation capacity (such as changes in O_3) along with appropriate meteorological condition. This conclusion corresponded well to the finding based on chemical transport model (Dai et al., 2023), which proposed strong chemical production of secondary aerosols when planetary boundary layer height was about 946.1m on O_3–$PM_{2.5}$ co-pollution days. The strong chemical productions in the oxidative atmosphere at medium MLH condition may overcome the dilution effect on $PM_{2.5}$ induced by mixing layer development, leading to higher $PM_{2.5}$ level at the ground level. However, it should be noted that the conclusions in this work were only suitable to summertime regional observations, especially for warm and humid seasons. The conditions would be different in wintertime (much lower O_3 level). More extended observations in time and space should be needed in the future to further examine and better understand the complex interactions between MLH, air pollution, and chemical processing.

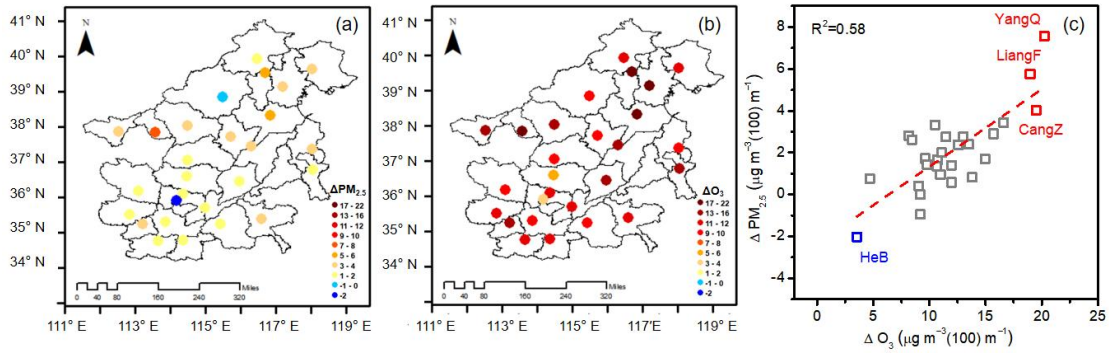

Figure 13. The spatial distribution of (a) $\Delta PM_{2.5}$ and (b) ΔO_3. (c) The relationships between $\Delta PM_{2.5}$ and ΔO_3 in the NCP during summertime. The corresponding correlation coefficients (R^2) was given at the top of the panel.

4 Conclusions

Mixing layer height (MLH) was generally considered as a critical physical parameter in

atmospheric environmental evaluation. It is assumed that extended mixing layer may lead to the dilution of air pollutants and thus tend to decrease surface concentrations. Several publications have indeed reported such anti-correlations in cold seasons. However, the understanding of the interaction between near surface O_3 and $PM_{2.5}$ (including its major components) along with the evolution of mixing layer during warm seasons remained poor. Furthermore, previous observational studies were mostly limited to a specific city. This paper is devoted to these topics by examining the response of MDA8 O_3, $PM_{2.5}$, and its major components to the changes in mixing layer meteorology in the North China Plain (NCP) during summertime. We showed that MDA8 O_3 initially increased and then decreased with the growth of MLH. The maximum turning point of MLH was around 900–1800 m. As for near-ground $PM_{2.5}$, similar non-linear change profile was found, with the maximum value of 31.65 μg m^{-3} under medium MLH condition (900–1200 m), which was quite different from the results conducted in cold seasons. Compared with winter, the occurrence of low MLH during summertime in the NCP was mostly accompanied with cloudy or rainy conditions, which promoted wet deposition and led to low concentrations of $PM_{2.5}$ at the ground level. Under medium MLH condition, strong chemical productions of SO_4^{2-} and OC occurred along with appropriate mixing layer meteorology, where RH was around 50−70 %, and the availability of atmospheric oxidants (i.e., O_3) increased. The strong chemical productions at medium MLH conditions may offset the diffusion effect on $PM_{2.5}$ induced by mixing layer development, resulting in higher $PM_{2.5}$ levels. The chemical characteristics of $PM_{2.5}$ significantly changed along with the growth of MLH. The composited concentration of NO_3^- was the highest under low MLH condition, while the composited concentrations of SO_4^{2-} and OC obviously increased under medium MLH condition. Temperature was the key factor controlling the opposite changes in NO_3^- and SO_4^{2-} concentrations in $PM_{2.5}$. We conclude that the MLH can be an indicator of air pollutants in cold seasons, but the correlation between MLH and air pollutants, such as O_3 and $PM_{2.5}$, should be treated with care in hot seasons. At least for the observation period in the NCP this was not the case. Although several studies have examined the change characteristics of MLH and its influence on ground-level O_3 and $PM_{2.5}$, it remains challenging to elucidate the mechanism underlying the complex relationships. In this work, we did not quantify the sensitivity of O_3 and $PM_{2.5}$ to different meteorological factors and chemical processes. To better understand the complex interactions between MLH, air pollution, and chemical processing, a more detailed consideration the aids of explicit models should be needed in the future. We also note that the present study was only confined to summertime

conditions (including two summer months) in the NCP, and the conclusions is likely to be different in other seasons and regions. Thus, more extended observations in time and space should be needed in the future.

Data availability. The data used in this paper can be provided upon request from the corresponding author.

Author contributions. J W and J G conceived the study and designed the experiments. **J W, F C, X Y,Y Y, L L and Y X** analyzed the data. **J W** prepared the manuscript and all the coauthors helped improve the manuscript.

Competing interests. The authors declare that they have no conflict of interest.

Acknowledgement. We thank the platform of National Atmospheric Particulate Chemical-Speciation-Network for making the $PM_{2.5}$ chemical composition data available.

Financial support. This work was supported by the National Natural Science Foundation of China (No. 42075182), the National research program for key issues in air pollution control (DQGG2021101) and the Central Level, Scientific Research Institutes for Basic R&D Special Fund Business, China (No. 2022YSKY-26).

582 **Reference**

583 Cheng, J., Su, J., Cui, T., Li, X., Dong, X., Sun, F., Yang, Y., Tong, D., Zheng, Y., Li, Y., Li, J., Zhang,
584 Q., and He, K.: Dominant role of emission reduction in $PM_{2.5}$ air quality improvement in Beijing
585 during 2013–2017: a model-based decomposition analysis, Atmos. Chem. Phys., 19, 6125-6146,
586 10.5194/acp-19-6125-2019, 2019.
587 Chow, W. S., Liao, K., Huang, X. H. H., Leung, K. F., Lau, A. K. H., and Yu, J. Z.: Measurement report:
588 The 10-year trend of $PM_{2.5}$ major components and source tracers from 2008 to 2017 in an urban site
589 of Hong Kong, China, Atmos. Chem. Phys., 22, 11557-11577, 10.5194/acp-22-11557-2022, 2022.
590 Chu, B., Ma, Q., Liu, J., Ma, J., Zhang, P., Chen, T., Feng, Q., Wang, C., Yang, N., Ma, H., Ma, J.,
591 Russell, A. G., and He, H.: Air Pollutant Correlations in China: Secondary Air Pollutant Responses
592 to NOx and SO_2 Control, Environ. Sci. Technol. Let., 7, 695-700, 10.1021/acs.estlett.0c00403, 2020.
593 Cohen, A. J., Brauer, M., Burnett, R., Anderson, H. R., Frostad, J., Estep, K., Balakrishnan, K.,
594 Brunekreef, B., Dandona, L., and Dandona, R.: Estimates and 25-year trends of the global burden of
595 disease attributable to ambient air pollution: an analysis of data from the Global Burden of Diseases
596 Study 2015, Lancet, 2017.
597 Dai, H., Liao, H., Li, K., Yue, X., Yang, Y., Zhu, J., Jin, J., Li, B., and Jiang, X.: Composited analyses
598 of the chemical and physical characteristics of co-polluted days by ozone and $PM_{2.5}$ over 2013–2020
599 in the Beijing–Tianjin–Hebei region, Atmos. Chem. Phys., 23, 23-39, 10.5194/acp-23-23-2023,
600 2023.
601 Dang, R., Liao, H., and Fu, Y.: Quantifying the anthropogenic and meteorological influences on
602 summertime surface ozone in China over 2012–2017, Sci. Total. Environ., 754, 142394,
603 10.1016/j.scitotenv.2020.142394, 2021.
604 Dawson, J. P., Adams, P. J., and Pandis, S. N.: Sensitivity of $PM_{2.5}$ to climate in the Eastern US: a
605 modeling case study, Atmos. Chem. Phys., 7, 4295-4309, 10.5194/acp-7-4295-2007, 2007.
606 Dian, J., Seidel, Chi, O., Ao, and, Kun, and Li: Estimating climatological planetary boundary layer
607 heights from radiosonde observations: Comparison of methods and uncertainty analysis, J. Geophys.
608 Res. Atmos., 10.1029/2009JD013680, 2010.
609 Du, C., Liu, S., Yu, X., Li, X., Chen, C., Peng, Y., Dong, Y., Dong, Z., and Wang, F.: Urban boundary
610 layer height characteristics and relationship with particulate matter mass concentrations in Xi'an,

611 Central China, Aerosol Air Qual. Res., 13, 1598-1607, 10.4209/aaqr.2012.10.0274, 2013.
612 Gao, Y. and Ji, H.: Microscopic morphology and seasonal variation of health effect arising from heavy
613 metals in $PM_{2.5}$ and PM_{10}: One-year measurement in a densely populated area of urban Beijing,
614 Atmos. Res., 212, 213-226, https://doi.org/10.1016/j.atmosres.2018.04.027, 2018.
615 Geiß, A., Wiegner, M., Bonn, B., Schäfer, K., Forkel, R., von Schneidemesser, E., Münkel, C., Chan, K.
616 L., and Nothard, R.: Mixing layer height as an indicator for urban air quality?, Atmos. Meas. Tech.,
617 10.5194/amt-2017-53, 2017.
618 Haman, C. L., Couzo, E., Flynn, J. H., Vizuete, W., Heffron, B., and Lefer, B. L.: Relationship between
619 boundary layer heights and growth rates with ground-level ozone in Houston, Texas, J. Geophys. Res.
620 Atmos., 119, 6230-6245, 10.1002/2013jd020473, 2014.
621 Haugen, D. A., Kaimal, J. C., Bradley, E. F.: An experimental study of Reynolds stress and heat flux in
622 the atmospheric surface layer, Q. J. Roy. Meteor. Soc., 97, 168-180, 1971.
623 Hou, P. and Wu, S.: Long-term changes in extreme air pollution meteorology and the implications for
624 air quality, Sci. Rep., 6, 23792, 10.1038/srep23792, 2016.
625 Jiang, N., Li, L., Wang, S., Li, Q., Dong, Z., Duan, S., Zhang, R., and Li, S.: Variation tendency of
626 pollution characterization, sources, and health risks of $PM_{2.5}$-bound polycyclic aromatic
627 hydrocarbons in an emerging megacity in China: Based on three-year data, Atmos. Res., 217, 81-92,
628 2018.
629 Kang, M., Zhang, J., Zhang, H., and Ying, Q.: On the relevancy of observed ozone increase during
630 COVID-19 lockdown to summertime ozone and $PM_{2.5}$ control policies in China, Environ. Sci.
631 Technol. Let., 8, 289-294, 10.1021/acs.estlett.1c00036, 2021.
632 Kong, L., Du, C., Zhanzakova, A., Cheng, T., and Zhang, S.: Trends in heterogeneous aqueous reaction
633 in continuous haze episodes in suburban Shanghai: An in-depth case study, Sci. Total Environ., 634,
634 1192, 10.1016/j.scitotenv.2018.04.086, 2018.
635 Li, J., Cai, J., Zhang, M., Liu, H., Han, X., Cai, X., and Xu, Y.: Model analysis of meteorology and
636 emission impacts on springtime surface ozone in Shandong, Sci. Total. Environ., 771, 144784,
637 https://doi.org/10.1016/j.scitotenv.2020.144784, 2021.
638 Liu, J., Wu, D., Fan, S., Mao, X., and Chen, H.: A one-year, on-line, multi-site observational study on
639 water-soluble inorganic ions in $PM_{2.5}$ over the Pearl River Delta region, China, Sci. Total Environ.,
640 601-602, 1720-1732, https://doi.org/10.1016/j.scitotenv.2017.06.039, 2017a.

Liu, P., Ye, C., Xue, C., Zhang, C., Mu, Y., and Sun, X.: Formation mechanisms of atmospheric nitrate and sulfate during the winter haze pollution periods in Beijing: gas-phase, heterogeneous and aqueous-phase chemistry, Atmos. Chem. Phys., 20, 4153-4165, 10.5194/acp-20-4153-2020, 2020.

Liu, T., Gong, S., He, J., Yu, M., and Zhao, Q.: Attributions of meteorological and emission factors to the 2015 winter severe haze pollution episodes in China's Jing-Jin-Ji area, Atmos. Chem. Phys., 17, 2971-2980, 10.5194/acp-17-2971-2017, 2017b.

Lou, M., Guo, J., Wang, L., Xu, H., Chen, D., Miao, Y., Lv, Y., Li, Y., Guo, X., Ma, S., and Li, J.: On the relationship between aerosol and boundary layer height in summer in China under different thermodynamic conditions, Earth Space Sci., 6, 887-901, 10.1029/2019ea000620, 2019.

Lu, M., Tang, X., Wang, Z., Wu, L., Chen, X., Liang, S., Zhou, H., Wu, H., Hu, K., Shen, L., Yu, J., and Zhu, J.: Investigating the transport mechanism of $PM_{2.5}$ pollution during January 2014 in Wuhan, Central China, Adv. Atmos. Sci., 36, 1217-1234, 10.1007/s00376-019-8260-5, 2019.

Ma, S., Shao, M., Zhang, Y., Dai, Q., and Xie, M.: Sensitivity of $PM_{2.5}$ and O_3 pollution episodes to meteorological factors over the North China Plain, Sci. Total. Environ., 792, 148474, 10.1016/j.scitotenv.2021.148474, 2021.

Markovic, M. Z., VandenBoer, T. C., and Murphy, J. G.: Characterization and optimization of an online system for the simultaneous measurement of atmospheric water-soluble constituents in the gas and particle phases, J. Environ. Monit., 14, 1872-1884, 10.1039/c2em00004k, 2012.

Miao, Y., Che, H., Zhang, X., and Liu, S.: Relationship between summertime concurring $PM_{2.5}$ and O_3 pollution and boundary layer height differs between Beijing and Shanghai, China, Environ. Pollut., 268, 115775, 10.1016/j.envpol.2020.115775, 2021.

Murthy, B. S., Latha, R., Tiwari, A., Rathod, A., Singh, S., and Beig, G.: Impact of mixing layer height on air quality in winter, J. Atmos. Sol.-Terr. Phy., 197, 10.1016/j.jastp.2019.105157, 2020.

NASTRO (The North American Research Strategy for Tropospheric Ozone): An assessment of tropospheric ozone pollution: a North American perspective , 2000.

Niu, T., Wang, J., Yang, Y., Wang, Y., and Chen, C.: A study on parameterization of the Beijing winter heavy haze events associated with height of pollution mixing layer, Adv. Meteorol., 2017, 1-11, 10.1155/2017/8971236, 2017.

Pan, L., Xu, J., Tie, X., Mao, X., Gao, W., and Chang, L.: Long-term measurements of planetary boundary layer height and interactions with $PM_{2.5}$ in Shanghai, China, Atmos. Pollut. Res., 10,

989-996, 10.1016/j.apr.2019.01.007, 2019.

Pang, N., Gao, J., Che, F., Ma, T., Liu, S., Yang, Y., Zhao, P., Yuan, J., Liu, J., Xu, Z., and Chai, F.: Cause of $PM_{2.5}$ pollution during the 2016–2017 heating season in Beijing, Tianjin, and Langfang, China, J. Environ. Sci. (China), 95, 201-209, 10.1016/j.jes.2020.03.024, 2020.

Park, S. S., Jung, S. A., Gong, B. J., Cho, S. Y., and Lee, S. J.: Characteristics of $PM_{2.5}$ haze episodes revealed by highly time-resolved measurements at an air pollution monitoring supersite in Korea, Aerosol Air Qual. Res., 13, 957-976, 10.4209/aaqr.2012.07.0184, 2013.

Porter, W. C. and Heald, C. L.: The mechanisms and meteorological drivers of the summertime ozone–temperature relationship, Atmos. Chem. Phys., 19, 13367-13381, 10.5194/acp-19-13367-2019, 2019.

Reddy, K. K., Naja, M., Ojha, N., Mahesh, P., and Lal, S.: Influences of the boundary layer evolution on surface ozone variations at a tropical rural site in India, J. Earth Syst. Sci., 121, 911-922, 10.1007/s12040-012-0200-z, 2012.

Rumsey, I. C., Cowen, K. A., Walker, J. T., Kelly, T. J., Hanft, E. A., Mishoe, K., Rogers, C., Proost, R., Beachley, G. M., Lear, G., Frelink, T., and Otjes, R. P.: An assessment of the performance of the Monitor for AeRosols and GAses in ambient air (MARGA): a semi-continuous method for soluble compounds, Atmos. Chem. Phys., 14, 5639-5658, 10.5194/acp-14-5639-2014, 2014.

Seinfeld, J. H. and Pandis, S. N.: Atmospheric Chemistry and Physics: From Air Pollution to Climate Change, . 2nd ed.; J. Wiley: Hoboken, N.J.,, p xxviii, 1203 p., 2006.

Steiner, Allison, L., Davis, Adam, J., Sillman, Sanford, Owen, Robert, C., Michalak, and Anna, M.: Observed suppression of ozone formation at extremely high temperatures due to chemical and biophysical feedbacks Proc. Natl. Acad. Sci. U. S. A., 107, 19685–19690, 2010.

Stull, R.: An Introduction to Boundary Layer Meteorology, Kluwer Academic Publishers, Dordrecht, the Netherlands, 1988.

Wang, F., Wang, W., Wang, Z., Zhang, Z., Feng, Y., Russell, A. G., and Shi, G.: Drivers of $PM_{2.5}$–O_3 co-pollution: from the perspective of reactive nitrogen conversion pathways in atmospheric nitrogen cycling, Sci. Bull. (Beijing), 67, 1833-1836, 10.1016/j.scib.2022.08.016, 2022a.

Wang, J., Bian, L., Xiao, C.: Dynamics of ekman boundary layer over the antarctic plateau in summer, Chinese Sci. Bull., 59, 999–1005, 2014.

Wang, J., Yang, Y.: Modern weather engineering. Meteorological Press, Beijing, 334–339, 2000.

Wang, J., Yang, Y., Zhang, X., Liu, H., Che, H., Shen, X., and Wang, Y.: On the influence of atmospheric super-saturation layer on China's heavy haze-fog events, Atmos. Environ., 171, 261-271, https://doi.org/10.1016/j.atmosenv.2017.10.034, 2017.

Wang, J., Gao, J., Che, F., Wang, Y., Lin, P., and Zhang, Y.: Dramatic changes in aerosol composition during the 2016–2020 heating seasons in Beijing–Tianjin–Hebei region and its surrounding areas: The role of primary pollutants and secondary aerosol formation, Sci. Total. Environ., 849, 157621, 10.1016/j.scitotenv.2022.157621, 2022b.

Wang, J., Yang, Y., Jiang, X., Wang, D., Zhong, J., and Wang, Y.: Observational study of the $PM_{2.5}$ and O_3 superposition-composite pollution event during spring 2020 in Beijing associated with the water vapor conveyor belt in the northern hemisphere, Atmos. Environ., 272, 10.1016/j.atmosenv.2022.118966, 2022c.

Wang, M., Duan, Y., Xu, W., Wang, Q., Zhang, Z., Yuan, Q., Li, X., Han, S., Tong, H., Huo, J., Chen, J., Gao, S., Wu, Z., Cui, L., Huang, Y., Xiu, G., Cao, J., Fu, Q., and Lee, S.-c.: Measurement report: Characterisation and sources of the secondary organic carbon in a Chinese megacity over 5 years from 2016 to 2020, Atmos. Chem. Phys., 22, 12789-12802, 10.5194/acp-22-12789-2022, 2022d.

Wang, X., Xiang, Y., Liu, W., Lv, L., Dong, Y., Fan, G., Ou, J., and Zhang, T.: Vertical profiles and regional transport of ozone and aerosols in the Yangtze River Delta during the 2016 G20 summit based on multiple lidars, Atmos. Environ., 259, 10.1016/j.atmosenv.2021.118506, 2021.

Wen, L., Xue, L., Wang, X., Xu, C., Chen, T., Yang, L., Wang, T., Zhang, Q., and Wang, W.: Summertime fine particulate nitrate pollution in the North China Plain: increasing trends, formation mechanisms and implications for control policy, Atmos. Chem. Phys., 18, 11261-11275, 10.5194/acp-18-11261-2018, 2018.

World Health Organization. WHO global air quality guidelines: particulate matter ($PM_{2.5}$ and PM_{10}), ozone, nitrogen dioxide, sulfur dioxide and carbon monoxide. Geneva: World Health Organization, 2021.

Wu, W. and Wang, T.: On the performance of a semi-continuous $PM_{2.5}$ sulphate and nitrate instrument under high loadings of particulate and sulphur dioxide, Atmos. Environ., 41, 5442-5451, https://doi.org/10.1016/j.atmosenv.2007.02.025, 2007.

Wu, X., Xin, J., Zhang, W., Gao, W., Ma, Y., Ma, Y., Wen, T., Liu, Z., Hu, B., Wang, Y., and Wang, L.: Variation characteristics of air combined pollution in Beijing City, Atmos. Res., 274,

731 10.1016/j.atmosres.2022.106197, 2022.
732 Xu, X., Zhang, H., Lin, W., Wang, Y., Xu, W., and Jia, S.: First simultaneous measurements of
733 peroxyacetyl nitrate (PAN) and ozone at Nam Co in the central Tibetan Plateau: impacts from the
734 PBL evolution and transport processes, Atmos. Chem. Phys., 18, 5199-5217,
735 10.5194/acp-18-5199-2018, 2018.
736 Yu, S.: Fog geoengineering to abate local ozone pollution at ground level by enhancing air moisture,
737 Environ. Chem. Lett., 17, 565-580, 10.1007/s10311-018-0809-5, 2019.
738 Zhang, G., Bian, L., Wang, J., Yang, Y., Yao, W., Xu, X.: The boundary layer characteristics in the
739 heavy fog formation process over Beijing and its adjacent areas, Sci. China Earth Sci., 48, 88–101,
740 2005.
741 Zhang, H., Wang, Y., Hu, J., Ying, Q., and Hu, X.-M.: Relationships between meteorological
742 parameters and criteria air pollutants in three megacities in China, Environmental Research, 140,
743 242-254, https://doi.org/10.1016/j.envres.2015.04.004, 2015a.
744 Zhang, R., Wang, G., Guo, S., Zamora, M. L., Ying, Q., Lin, Y., Wang, W., Hu, M., and Wang, Y.:
745 Formation of urban fine particulate matter, Chem. Rev., 115, 3803-3855,
746 10.1021/acs.chemrev.5b00067, 2015b.
747 Zhang, X., Xiao, X., Wang, F., Brasseur, G., Chen, S., Wang, J., and Gao, M.: Observed sensitivities of
748 $PM_{2.5}$ and O_3 extremes to meteorological conditions in China and implications for the future,
749 Environ. Int., 168, 107428, 10.1016/j.envint.2022.107428, 2022.
750 Zhao, W., Tang, G., Yu, H., Yang, Y., Wang, Y., Wang, L., An, J., Gao, W., Hu, B., Cheng, M., An, X.,
751 Li, X., and Wang, Y.: Evolution of boundary layer ozone in Shijiazhuang, a suburban site on the
752 North China Plain, J. Environ. Sci. (China), 83, 152-160, 10.1016/j.jes.2019.02.016, 2019.
753 Zhu, X., Tang, G., Guo, J., Hu, B., Song, T., Wang, L., Xin, J., Gao, W., Münkel, C., Schäfer, K., Li, X.,
754 and Wang, Y.: Mixing layer height on the North China Plain and meteorological evidence of serious
755 air pollution in southern Hebei, Atmos. Chem. Phys., 18, 4897-4910, 10.5194/acp-18-4897-2018,
756 2018.
757